Graphene oxide nanocomposite hydrogel beads for removal of selenium in contaminated water

Pasan Chinthana Bandara,[†] Jem Valerie D. Perez,[†] Enrico Tapire Nadres,[†] Raj Gopal Nannapaneni,[†] Konrad J. Krakowiak[†] and Debora Frigi Rodrigues[†,]*

[†]Department of Civil and Environmental Engineering, University of Houston, Houston, TX 77204-4003. Email: dfrigirodrigues@uh.edu

ABSTRACT

Selenium in water is becoming of increasing risk to human exposure, because only recently serious health effects have been associated to their presence in water resources. The present study investigated the development and optimization of the composition of graphene oxide polymeric nanocomposite hydrogel beads using response surface methodology. The use of polymers such as chitosan and polyethyleneimine, which are rich in amine and alcoholic functional groups, provided enhanced removal of anionic selenium species from the water. Experimentally validated polymeric beads were used to perform batch adsorptions of selenium under different conditions such as pH, bead dosage, and diverse selenium concentrations to investigate their potential use, adsorption kinetics, and selenium removal mechanisms. Acidic conditions were found to best remove negatively charged selenium ions from aqueous solutions via -OH, -COOH, and amine functional groups present in the beads. The adsorption kinetic mechanism was better described by the pseudo-second order adsorption kinetic, indicating that the beads remove selenium via chemisorption mechanisms. The isotherm studies showed an adsorption capacity of 1.62 mg/g based on the Langmuir isotherms at 25 ºC. Regeneration studies showed loss of available adsorption sites after the first desorption treatment with different concentrations of NaOH and HCl. The mathematically optimized nanocomposite was further used to treat selenium spiked in real environmental water samples, which confirmed that the best removal of selenium occurs in acidic conditions.

Keywords - Selenium, response surface methodology, hydrogel beads, nanocomposites, graphene oxide

1. INTRODUCTION

In recent studies, graphene oxide (GO) has shown a great potential for incorporation in polymeric materials to develop a more stable, efficient, and effective, multi-functional class of polymer nanocomposites for various water related applications.[1-5] This advancement has several advantages rather than using a singular material, such as enhanced adsorption capacity, widened selectivity of contaminants and more importantly, the increased potential for large-scale fabrication.[6-7] The main goal of this investigation was to optimize the composition of chitosan-polyethyleneimine-graphene oxide (CS-PEI-GO) hydrogel beads for enhanced removal of selenium through surface adsorption mechanisms.

Chitosan (CS) is an abundant biopolymer produced from chitin, which is obtained from the shells of shrimp. Its composition can be expressed as poly(b-1-4)-2-amino-2-deoxy-D-glucopyranose, with the repeating unit including glucosamine subunits and amine functional groups.[8] CS has attracted much attention as it is known to possess efficient adsorption capabilities due to the presence of amino and hydroxyl functional groups.[9-11] These amine groups can uptake negatively charged ions via electrostatic attractions.[1, 11] Chitosan is hydrophilic and dissolves in slightly acidic solutions (pH<6.5). At pH values below 6.5, amine functional groups get protonated easily to accompany metal removal. However, CS itself lacks structural strength; therefore, making it unsuitable to be used as it is in water related applications. Therefore, CS is often incorporated with matrices of other materials, such as GO, other polymers or crosslinking agents, which assist in providing structural stability.[1,12] CS has shown to remove heavy metals such as chromium, copper, and lead in previous studies.[1, 8, 10, 13-14]

Polyethyleneimine (PEI) is a synthetic polycation, which is formed using polymerization of iminoethylene monomers. PEI is a rich source of primary, secondary and tertiary amines, low in toxicity and odorless, which paves the way for its wide applications. In this study, PEI is used as subordinate polymeric material alongside with CS as the crosslinking process to prepare the polymer beads consumes some of the amine groups found on CS, hence reducing its adsorption capacity. PEI not only accounts for the loss of amine groups during the crosslinking process, but also brings in enhanced removal capacities. [15-17]

In this work, beads containing CS-PEI-GO were developed to be employed in batch or in packed bed columns for water treatment approaches. The selection of the amount of each polymer and nanomaterial in the composition of the nanocomposite beads was mathematically modelled using the Box-Behnken Design (BBD) within the response surface methodology. In the present investigation, BBD was employed due to its flexibility in providing better and sufficient understanding about a system that has limited number of independent factors and a single response factor.[1] The beads produced were investigated for the removal of Selenium.

In the last decades, increasing interest has been growing for addressing selenium (Se) contamination. Selenium exists naturally in soils in various polymorphs. Selenate, Se(VI), is the most soluble of them all, followed by selenite, Se(IV).[18-20] Apart from being a natural contaminant like arsenic, there are studies showing excessive selenium concentrations measured in close proximity to oil-gas wells.[18, 21-22] Several studies from places over the globe, such as lower Arkansas river valley in Colorado, USA[23], San Joaquin Valley in California, USA,(Biogeo) Amman Zarqa basin in Jordan[24], northern Italy[25-26], southwestern Nigeria[23] and Hokkaido, Japan [27-28] suggest that industrial activities, such as mining, road development

projects, and petrochemical processes have a strong impact on exceeding safety levels of Se in water bodies.[18, 22, 27-31]

Selenium is regulated under the national drinking water standards, at maximum contaminant level (MCL) and maximum contaminant level goal (MCLG) values of 0.05 ppm, for being known to cause hair or fingernail loss, numbness in fingers or toes and circulatory problems. [29] It has also been associated with reproductive irregularities, juvenile mortalities, physical impairments in aquatic species, and livestock.[18, 32-35] EPA identifies petroleum and metal refineries, as well as leaching out of natural deposits, as major sources of increasing selenium contamination. However, chronic effects of selenium on human health has been an understudied field.[21, 33, 35-36] Initial studies have shown that selenium can be a potential human carcinogenic and present teratogenic species, however very few studies have investigated the removal of such contaminant though the literature describes the adsorbents such as metal–organic framework-based materials, magnetite-based nanomaterials, carbonaceous nanomaterials and polymer-based nanomaterials for selenium adsorption from contaminated waters.[37-41] Therefore, approaches to remove such emerging contaminant is still in great need, which led us to develop a novel polymer nanocomposite bead for the removal of selenium. In this work, we investigated a novel approach to remove selenium from water using graphene oxide-based nanocomposite hydrogel beads as recent studies shows the potential of such assemblies for water related applications such as water treatment and contaminant removal.[1, 42-46]

2. EXPERIMENTAL SECTION

2.1 Materials and methods. The following chemical grade reagents were used in the synthesis and processing: graphite (<45μm), chitosan (low molecular weight), polyethyleneimine (50%

(wt/wt%) in water, avg. MW 750,000), glutaraldehyde (25% (wt/wt%) in water), selenous acid (H_2SeO_3, 97.0% assay) for Se solutions, sodium hydroxide (NaOH, ACS reagent, ≥ 97% assay, pellets), nitric acid (HNO_3, ACS reagent, 70% assay), and hydrochloric acid (HCl, ACS reagent, 37% assay). They were all purchased from Sigma Aldrich. The modified Hummer's method was employed to synthesize GO used in the processing of the bead.[1, 47] The details on GO characterization can be found in our previous publication.[48] All the solutions were prepared using deionized (DI) water unless specified otherwise.[49]

2.2 Preparation of working solutions. For the synthesis of the CS-PEI-GO mixtures, stock solutions of 4% CS solution was prepared by dissolving 4 g of CS in 96 g of 2% HCl prepared in DI water. A concentration of 30% PEI was prepared by dissolving 60 g of 50% PEI in 40 g of 2% HCl, and 5000 ppm GO was prepared in DI water and sonicated for 15 min. Different working mixtures, as described in the ESI table S1, were prepared by using these stock solutions. A stock solution of 500 ppm concentration of Se(IV) was prepared using H_2SeO_3 in DI water to be used for the batch adsorption at the desired concentrations as described below. For the dynamic contact experiments involved in the optimization step, the pH of selenium solutions was not adjusted. For the kinetic experiments, pH was adjusted to the optimum pH identified in the section 2.8 described below.

2.3 Experimental design using RSM. The statistical design software Design Expert 11.0 from Stat-Ease Inc. (Minneapolis, USA) was used to develop the mixture design. In this design, four variables (X_i), namely PEI composition *(X_1)*, GO composition *(X_2)*, and GLA composition *(X_3)* were used as independent factors to create 15 design points based on a single response variable (Y_i): Se % removal *(Y_1)* using a three-level Box-Behnken Design.[1] Independent experimental variables and their factor levels are provided in the electronic supporting information (ESI) table

S1. The selection of the independent variables were pre-determined based on preliminary, studies which demonstrated successful and efficient synthesis of the beads.[1, 48]

2.4 Preparation of nanocomposite beads. Overall summary of the preparation and characterization is presented in Figure 1. CS–PEI–GO beads were prepared according to compositions described in ESI table S2. Required weights of CS, GO and PEI stock solutions were mixed in glass vials overnight. The homogenized CS-PEI-GO solution was placed in a 10 mL syringe with 23G needle and fixed to a syringe pump with a 1 mL/min feed rate and dropped onto a 1.5 M NaOH solution. The NaOH solution was stirred at 150 rpm to avoid the aggregation of beads. At the end of this step, beads were separated from the NaOH solution, and washed with DI water to remove basicity. The washing continued several times until the pH of the washings became neutral. Next, the beads were cross-linked for 30 min with the required concentration of GLA solution for each design point as mentioned in ESI table S1. Beads were washed again with DI water to remove excess GLA. Finally, they were stored in DI water until used for the batch adsorption and characterization.

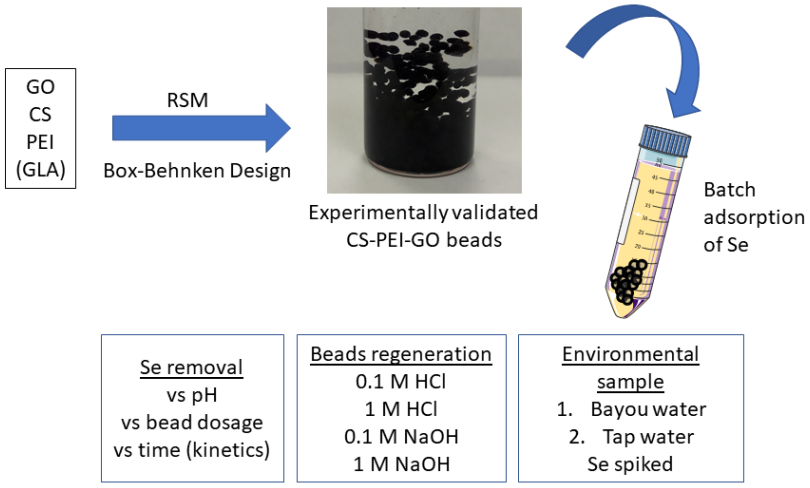

Figure 1: Preparation and characterization of Graphene oxide nanocomposite hydrogel beads, as well as analyzes performed on the beads.

2.5 Selenium removal experiments. Batch adsorption of 20 mL aliquots of 10 ppm Se solutions with 0.5 g of beads was carried out at 25 ºC temperature for 24 h. Batches were shaken at 150 rpm to allow maximum contact between beads and the solution and to avoid settling down of the beads. After the adsorption reached equilibrium, the supernatant was collected and filtered with 0.2 µm polyethersulfone (PES) syringe filters (25 cm diameter) to remove any leftover beads. Samples were diluted in 2% nitric acid and analysed with Thermo Scientific icap RQ inductively coupled plasma mass spectrometry (ICP-MS) to quantify the selenium concentration in the samples. The eq 1 was used to calculate the percentage Se removal.

$$\%\ Se\ Removal = \frac{Initial\ conc. - Final\ conc.}{Initial\ conc.} \times 100\% \qquad (1)$$

2.6 Modelling analysis for composition optimization of the beads. The Design Expert software 11.0 was used to carry out the modelling analysis for percentage Se removals. Experimental data were fitted into a general quadratic equation,

$$Yi = \beta_0 + \sum_{i=1}^{n} \beta_i x_i + \sum_{i=1}^{n-1} \sum_{j=i+1}^{n} \beta_{ij} x_i x_j + \sum_{i=1}^{n} \beta_{ii} x_i^2 \qquad (2)$$

where β_0, β_i, β_{ij}, and β_{ii} are the coefficients for offset, linear effect, interaction effect, and quadratic effect, respectively. Analysis of variance (ANOVA) technique was used to assess the significance of each model term and overall models, which was later subjected to statistical analysis, surface analysis, and numerical optimization in order to identify an optimized solution for the bead composition. The final CS-PEI-GO bead composition was synthesized based on the suggested optimum concentrations for each component as determined by the model. Then, the Se

164 removal experiments were performed in order to experimentally validate the suggested optimum
165 solution from the RSM model. Beads containing CS only, CS-PEI only and CS-GO only beads
166 were used as negative controls for the validation experiments. CS, PEI and GO concentrations in
167 the negative controls were the same as the mathematically optimized solution from RSM. GLA
168 concentration was used to crosslink all the negative control beads in a similar fashion as the CS-
169 PEI-GO optimum composite. Experimentally validated beads were characterized and further
170 analyzed for their removal trends, adsorption kinetics, and regeneration.

171 **2.7 Characterization of mathematically optimized beads.** Successful synthesis and functional
172 properties of optimized and validated beads were investigated using scanning electron
173 microscopy (SEM), X-ray powder diffraction (XRD), attenuated total reflectance - infrared
174 (ATR-IR) spectroscopy, and X-ray photoelectron spectroscopy (XPS). Bead samples were freeze
175 dried for 12 h and grounded prior to ATR-IR and XPS analyses, using a FreeZone Plus 4.5 Liter
176 cascade benchtop freeze-drier system at a collector temperature of -84 ºC. Freeze-dried beads
177 were attached to carbon double tape and coated with a thin gold layer using a Desk V sputter
178 (Denton Vacuum) prior to the SEM analysis. A Jeol JSM-6010LA (Jeol, Peabody, MA)
179 analytical scanning electron microscope was used to obtain the SEM images of the coated beads.
180 The X-ray diffraction pattern of CS-PEI-GO was obtained using a Rigaku MiniFlex600 benchtop
181 X-ray diffractometer with Cu source. Micromeritics 3Flex Brunauer–Emmett–Teller (BET)
182 instrument was used to obtain N_2 adsorption/desorption isotherms on the freeze-dried beads.
183 Prior to the measurements, all samples were degassed under vacuum at 120 ºC for 5 h. Obtained
184 data were used to estimate BET[50] specific surface area (SSA) and Barrett-Joyner-Halenda
185 (BJH)[51] pore size distribution. ATR-IR samples were collected using a Nicolet iS10 Mid Infrared
186 FTIR Spectrometer (Thermo Fisher Scientific, USA) under air as the background. Omnic 8

187 Software (Thermo Fisher Scientific, USA) was employed to process the acquired raw spectra and
188 prominent peaks were identified. XPS spectra were acquired using a PHI 5700 X-ray
189 photoelectron spectrometer as low- and high-resolution scans were done at pass energies of 23.5
190 and 187.8 eV respectively. Raw spectra were further processed using the MultiPak V7.0.1
191 (ULVAC-PHI, Inc.) and Origin Pro8.5 (OriginLab, Northampton, MA) packages.

192 **2.8 Role of pH and bead dosage on Selenium removal.** Optimized beads were used to perform
193 adsorption experiments by varying pH to identify the removal trends. Se solutions containing 10
194 ppm concentrations had the pH adjusted by adding 0.1 M HCl and 0.1 M NaOH to obtain Se
195 solutions with pH ranging from 3 to 8. Masses of the beads before and after the adsorption were
196 measured to assess the stability and recovery of the beads when exposed to the selected pH
197 ranges. An optimum pH was selected, based on significant Se removals to perform adsorption
198 experiments with varying bead dosage from 20 to 40 g/L. Treated samples were analysed with
199 ICP-MS and used to calculate the percentage removals and adsorption capacity. The best pH and
200 bead dosage based on the higher removal and adsorption capacity were used to carry out the
201 subsequent experiments.

202 Furthermore, the zeta potential of the beads over various pH values was investigated to
203 understand the potential Se removal mechanisms via electrostatic attractions. Firstly, 100 mg of
204 freeze-dried optimized CS-PEI-GO beads were ground into a fine powder and dispersed in 100
205 ml of DI water. Then the suspension was bath-sonicated for 6 h and stirred for 16 h at 150 rpm.
206 The suspension was allowed to settle for 16 h, after which, the supernatant containing suspended
207 bead particles was collected and then divided into several vials. The pH of each vial was adjusted
208 to pH 3-12 using 0.1 M HCl or NaOH and analysed using a Malvern ZEN 5600 Zetasizer.

Polystyrene vials with the refractive index of 1.59 was used in this analysis. All the experiments were done at the room temperature of 22 ºC.

2.9 Kinetics of Se removal using the optimized beads. To understand the adsorption kinetics of the optimized CS-PEI-GO beads, adsorption measurements were carried out at 25 °C. These studies were performed with initial Se concentrations of 2, 10 and 20 ppm. Samples were collected at time intervals from 0 to 24 hours. Pseudo-first order and pseudo-second order models were evaluated to fit the obtained adsorption data to understand its characteristics. Pseudo-first order model is expressed in a linear form as,

$$\ln(q_t - q_e) = ln(q_e) - k_1 t \quad (3)$$

where q_e and q_t are the amount of Se adsorbed per mass of adsorbent at equilibrium and at any time – t respectively, and k_1 is the first order rate constant.[52-53] Plots of $\ln(q_e\text{-}q_t)$ vs time were developed for each data set.

The slope and intercept were used to evaluate theoretical values of q_t and k_1. Similarly, pseudo-second order kinetic model is expressed in a linear form as,

$$\frac{t}{q_t} = \frac{1}{k_2 q_e^2} + \frac{1}{k_2} \quad (4)$$

where k_2 is the second order rate constant.[53-55] Plots of t/q_t vs time were developed for each adsorption data set and the slope and intercept were used to evaluate theoretical values of q_t and k_2. The kinetic model best describing the adsorption data was determined based on the goodness of fit, R^2. The agreement of theoretical and experimental q_e values was determined based on two tailed t-test at α=0.05.

2.10 Adsorption isotherm studies for Se removal using the optimized beads. Adsorption isotherms corresponding to the initial Se concentrations of 5 to 250 ppm at 25 ºC were obtained for the CS-PEI-GO beads. Similarly, adsorption experiments were done at 150 rpm for 24 hours and the initial pH of the samples and bead dosage were adjusted based on earlier findings. Obtained data were tested against the non-linear forms of Langmuir and Freundlich isotherm models, which are described below.

The non-linear form of Langmuir isotherm model is given by,

$$Q_e = \frac{Q_m b C_e}{1 + b C_e} \quad (5)$$

where, b (L/g) is the Langmuir equilibrium constant and Q_m is the monolayer saturation capacity.[53, 55] Also, the linear form of the Freundlich isotherm model is given by,

$$Q_e = K_F C_e^{1/n} \quad (6)$$

where, K_F (L/g) is the Freundlich constant and 1/n is the sorption intensity.[53, 55-56]

2.11 Regeneration of optimized beads. Regeneration of the beads was determined using the following desorption agents: 0.1 M HCl, 1 M HCl, 0.1 M NaOH, 1 M NaOH. First, the beads were used to perform adsorption experiment for 24 h at 25 °C with 10 ppm Se. Afterwards, used CS-PEI-GO beads were separated from the supernatant and were thoroughly washed with DI water in order to remove excess Se that did not get adsorbed. Then, the washed beads were added to 20 mL aliquots of different desorption agents and allowed to desorb at 150 rpm for 24 h at 25 °C. Treated beads were separated from the supernatant, and thoroughly washed with DI water to remove unused desorption agents. For the beads treated with HCl solutions, an additional treatment with 10 mL of 0.1 M NaOH for 45 min was performed in the beads in order

to deprotonate the amine groups on the surface. Later, they were washed thoroughly with excess DI water until the pH of the water was neutral. Washed beads were cyclically reused. In total, 4 cycles of adsorption-desorption experiments were done. Samples were collected at the end of each adsorption or desorption cycle and % adsorption and % desorption were calculated using the eq 7 and 8 respectively.

$$\% \, Adsorption = \frac{C_i - C_e}{C_i} \times 100 \quad (7)$$

$$\% \, Desorption = \frac{C_d}{C_i - C_e} \times 100\% \quad (8)$$

Here, C_i, C_e, and C_d are the measured concentrations of selenium in the supernatant before the adsorption, after the adsorption, and after the desorption, respectively.

2.12 Application of beads with environmental samples spiked with Se. Bayou water and tap water samples were collected, characterized, and spiked with 10 ppm Se for adsorption experiments to understand the behaviour of the beads, when applied in a real environmental water with different chemistries. Bayou water sample was collected from the Brays Bayou Greenway Trail, Houston, TX at the coordinates of 29.702314, -95.404883. The tap water sample was collected from the drinking water fountain in the Engineering Building 2, at the University of Houston, Houston TX. Both samples were collected in the spring when weather conditions were normal and free of overnight rains. Conductivity of the bayou water sample was 700 µs/cm with turbidity of 5.1 NTU and a pH of 7.4. Conductivity of the tap water sample was 370 µs/cm with turbidity of 0.3 NTU and a pH of 7.8. None of the samples contained detectable amounts of Se. The water samples were adjusted to the optimum pH for Se removal as determined earlier.

3. RESULTS AND DISCUSSION

3.1 Mathematical optimization of the model. The hydrogel bead composition was optimized using the Design expert software. The mixture design was prepared using the concentrations suggested by BBD. This method provides adequate flexibility to investigate the behavior of the three-factor system.[1] The design can be thought as a cube of which vertices, middle points of the edges and center point of the cube represent different combinations of the bead composition.[1] Obtained results from the batch adsorptions were fitted into the eq 2 to develop the initial model in the form of the quadratic equation. The resulting 2nd order equation for Se removal is presented as follows.

$$Y_i = 61 + 3.0X_1 + 2.5X_2 + 5.5X_3 - 1.8X_1X_2 - 2.0X_1X_3 + 0.5X_2X_3 + 8.5X_1^2 + 2.2X_2^2 - 2.0X_3^2 \quad (9)$$

ANOVA technique was employed to investigate the significance of each term in the unmodified model equation, based on the *p*-values. The original quadratic model gave an *F*-value of 6.43 and a *p*-value of 0.03 indicating that the model was significant. The model showed a R^2 of 0.92, which indicates the agreement between the actual and predicted responses as shown in the ESI figure S1a with no outliers present.[1, 57] As shown in the ESI figure S1b the residuals were distributed within a very narrow range, indicating that there were no outliers present, compared to the set limit of ± 3 standard deviations as indicated by the red horizontal lines. In summary, the diagnostic analysis showed that the obtained model is adequate for predicting Se removals effectively.

To improve the model, the non-significant terms were excluded from the original model by employing the backward calculation method. In this method, terms with p-values > 0.05 were removed from the model until a better-modified model equation was obtained. The new model is

given by the eq 10. Surface plots were used for the additional analysis of the model parameters as shown in ESI figure S2. They provide a platform to investigate the individual and combined effects of independent variables on the Se removal.

$$Y_i = 61 + 3.0X_1 + 2.5X_2 + 5.5X_3 - 8.5X_1^2 \qquad (10)$$

Figure S2 illustrates three surface plots for combinations of two independent variables for % Se removals; while the third independent variable is fixed at the highest level. In summary, the highest removals of Se was recorded in the region where all factors were at their highest range. This indicates that all the three independent factors did show a positive influence on the Se removal.

3.2 Experimental validation of mathematically optimized beads. An optimized solution for the amounts of GO, PEI and GLA were selected based on the desirability function, which was used as the objective function of the optimization as follows.

$$d_i(\text{desirability}) = \frac{(calculated\ y_i - minimum\ y_i)}{(maximum\ y_i - minimum\ y_i)} \qquad (11)$$

As the goal for the numerical optimization, Se removal was subjected to maximization. The obtained solution with the highest desirability function was selected for the experimental validation. Based on the optimization, the optimum bead composition for maximum Se removals of 81± 4% was predicted to be 1500 ppm GO, 2.0% PEI crosslinked with 2.5% GLA. These concentrations were used to synthesize beads as mentioned in the section 2.4, and Se removals were quantified. Control beads containing CS only, CS-PEI only and CS-GO only were also tested. ESI figure S3 shows the comparison of the optimized CS-PEI-GO beads experimentally and determined by the model for Se removals, along with the control beads.

Two tailed t-test at α=0.05 was performed to determine the statistical significance of the results obtained. Calculated *p* value of 0.36 indicated that there is no significant difference between the actual and the model predicted Se removals. Furthermore, the removal with CS-PEI-GO beads were tested with four different batches of beads and compared to the predicted removal. The results showed reproducibility of the bead preparation. Calculated *p* values of 0.0001 for the removals from CS-PEI-GO and CS-PEI only beads showed that the inclusion of GO into beads presented a statistically significant enhancement of the Se removal. This observation was further confirmed by the calculated *p value* of 0.0001 for the removals obtained with CS-GO and CS beads compared to CS-PEI-GO, indicating a significant difference in the obtained Se removals. Inclusion of GO showed enhanced selenium removals, which can be understood as GO is a rich source of functional groups such as -OH and -COOH, which can be protonated in acidic conditions leading to electrostatic attractions with the negatively charged Se species present in the solution as well as the higher surface area provided for contaminant adsorption.[58-59]

Following successful experimental validation, the beads were characterized and further analyzed for trends in Se removal.

3.3 Characterization of optimized beads.

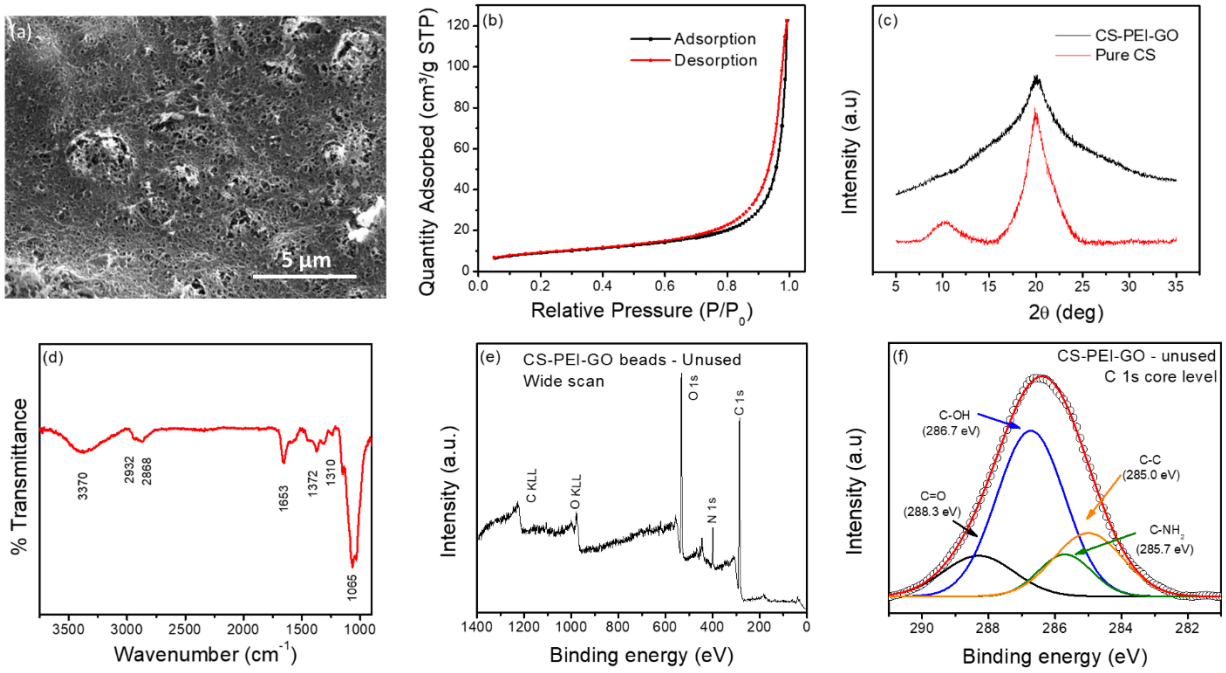

Figure 2. Detailed characterization of the optimized CS-PEI-GO nanocomposite beads: (a) SEM image showing the rough and porous surface of the CS-PEI-GO beads, (b) N_2 adsorption–desorption isotherms for optimized CS-PEI-GO beads, (c) XRD patterns of CS-PEI-GO and pure CS, (d) ATR-IR spectra of the CS-PEI-GO beads, XPS spectra showing (e) wide scan and (f) deconvolution of C1s core level.

The detailed characteristics of the optimized CS-PEI-GO beads are shown in the ESI figure S4a and figure 2. The SEM images of the beads showed the existence of a well-defined porous structure in the beads as given by figure 2a. N_2 adsorption–desorption isotherms obtained for CS–PEI–GO beads are shown in the figure 2b. Based on the IUPAC classification, the isotherm shape represents a type IV isotherm indicating the presence of a mesoporous structure with pore sizes between 2 and 50 nm.[60] BET standard plot was constructed for the p/p_0 range from 0.05 to 0.30 (ESI figure S4b). Based on the intercept and the slope, the estimated value of interaction constant was 101 and the monolayer adsorption capacity was estimated to be 3.24x10^{-}

^{4} mol/g. BET specific surface area was calculated as 32 m^2/g indicating the inclusion of GO resulted in increased specific surface as compared to that of pure chitosan; therefore creating more sites for Se adsorption.[61-63] The pore size distributions obtained based on the adsorption and desorption isotherms are shown in the ESI figure S4c indicating availability of mesopores as confirmed by the average BJH adsorption and desorption pore diameters of 27 nm and 25 nm.

As shown in the figure 2c, XRD patterns of CS-PEI-GO exhibited the peak at 2θ = 20.03º. This peak was broader compared to the XRD pattern of pure CS, which showed two peaks located at 2θ = 10.33° and 20.07º, indicating the decrease in crystallinity.[64-65] Interactions that took place between the various functional groups of CS-PEI-GO bead surface during the bead synthesis resulted in change of crystallinity[1] due to the expansion of the polymer network. Such expansion has shown to enhance the adsorption ability of the nanocomposites.[13, 66]

The ATR-IR spectra for the CS-PEI-GO beads (figure 2d) showed clear peaks at 1065, 1310, 1372, 1653, 2868, 2932 and a broad peak at 3370 cm^{-1}. The peak at 1050 cm^{-1} was assigned to C-N bonds originated from the PEI[67] and the peak at 1310 cm^{-1} was assigned to -CH_2 which originated from CS and PEI.[16, 21] The peak at 1372 cm^{-1} can be assigned to the C-N stretching vibrations from PEI and CS. In the results, it appeared that the signals from the primary amine groups may have overlapped with the peak at 1372 cm^{-1}.[1, 68] Next, the peak at 1653 cm^{-1} can be attributed to the carbonyl stretch of –NHCO– group, which originated from the crosslinking of amine groups with GLA.[1, 68] Two peaks at 2868 and 2932 cm^{-1} were attributed to the stretching vibrations from CH_2 and CH_3.[68] The broad peak at 3030-3600 cm^{-1} can be assigned to the OH from GO and CS or to the amine groups from CS and PEI. [1, 68] In the wide scan of the XPS of unused CS-PEI-GO beads (figure 2e), three major peaks can be identified at the binding energies of 286, 399 and 533 eV, which are attributed to C 1s, N 1s, and O 1s.[1, 13] The high-

resolution scan of the C1s core level of the CS-PEI-GO beads (figure 2f) showed the availability of -C-OH bonds and C=O with peaks at 286.7 and 288.3 eV, mainly resulting from the successful inclusion of GO. [69-71] Also, the peak at 285.7 eV assigned to C-NH_2 originated from the CS and PEI.[1, 13] Therefore, the characterization of the CS-PEI-GO beads indicated the presence of functional groups that are useful in adsorption of negatively charged particles, such as the selenium species used in the experiments in this study.

3.4 Selenium removal with pH and dosage. The trends of % Se removal and respective adsorption capacity of the beads with initial pH of 3 to 8 at 10 ppm Se solution are illustrated in figure 3a.

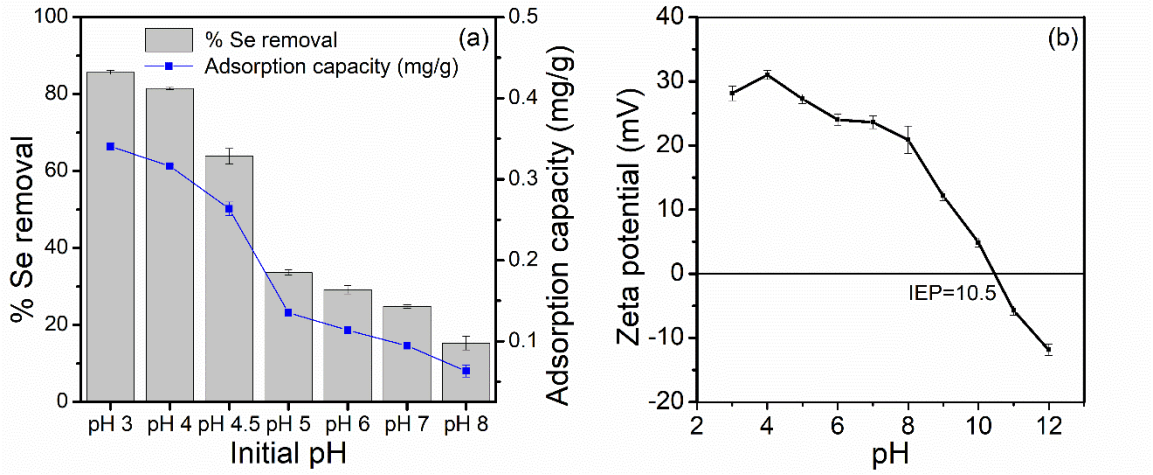

Figure 3. (a) Percentage Se removal and adsorption capacity (mg/g) with the initial pH of the Se solution and (b) zeta potential of the beads with varying pH indicating the favorable adsorption of negatively charged Se species in lower pH values.

The pH of the solution played a significant role in the removal of selenium. The % Se removal showed a significant drop with increasing pH values. On the other hand, increasing acidity also showed much better removals suggesting that acidic conditions are more suitable for Se uptake with the CS-PEI-GO beads. This can be understood as the dissolved selenious acid equilibrates in the solution as it disassociates to form $HSeO_3^-$ and H^+ making the solution acidic.

$$H_2SeO_3 \rightleftarrows H^+ + HSeO_3^- , \quad pK_{a1} = 2.46 \tag{12}$$

According to the above-mentioned dissociations, between pH 3.5 and 9.0, the $HSeO_3^-$ ion becomes more dominant as the ionic strength of the solution is high; therefore when the beads are introduced to the Se solution, functional groups such as -OH and -COOH become protonated leading to electrostatic attractions with the negatively charged Se species present in the solution.[58-59] The CS-PEI-GO nanocomposite beads have been previously shown to remove Cr(VI) and Cu(II) in acidic conditions where electrostatic attractions are meant to be the main mechanism of metal uptake.[1] Similarly, earlier studies have shown much better Se removals at lower pH values with carbonaceous and non-carbonaceous materials indicating that Se removals are typically favored by acidic conditions.[55-56, 58] When the ionic selenium species concentration in the solution get reduced due to the adsorption, pH increases as the equilibrium shift towards the left in eq 12, resulting in decreasing ionic strength. Furthermore resulting OH^- competes with the anionic selenium species for adsorption sites on the nanocomposite reducing the adsorption efficiency.[72-74] Based on the removals, pH 4 was selected to perform the subsequent experiments.

Zeta potential analysis of the optimized CS-PEI-GO beads over the pH range of 3-12 showed positive surface charge density of the adsorbent as shown in the figure 3b. Positive zeta

potentials were observed over a wide pH range, from acidic pH to the isoelectric point (IEP) of 10.5, indicating favorable conditions for formation of electrostatic attractions with anionic species. The observed IEP is above the IEP of chitosan and agrees with the earlier studies that has shown increments in IEP following the inclusion of PEI due to the large number of amine groups present.[75-76]

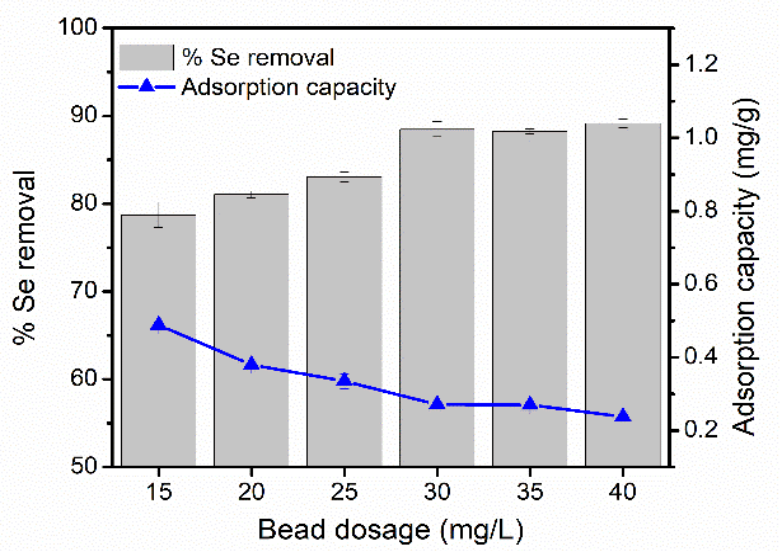

Figure 4. Percentage Se removal and adsorption capacity (mg/g) with bead dosage show a plateau in the percentage removals beyond 30 g/L bead dosage. This dosage was selected as the optimum dosage for the subsequent experiments.

The figure 4 shows the % Se removal with bead dosage. Bead dosages from 20- 40 g/L were tested to identify the trends and bead dosage for the following experiments. A significant increment in the % Se removal was shown with the increased bead dosage of 30g/L. Se removals reached a plateau afterward, as suggested by the obtained *p-value*s of 0.64 and 0.10 with the two tailed *t*-test at α=0.05 for the removals obtained with 30 g/L-35 g/L and 35g/L-40 g/L bead dosages, respectively. The increasing bead dosage allowed increasing availability of the functional groups for more adsorption; however, beyond the dosage of 30g/L the Se uptake did

not increase significantly. Therefore, the dosage of 30g/L was selected as the most suitable dosage for the next experiments.

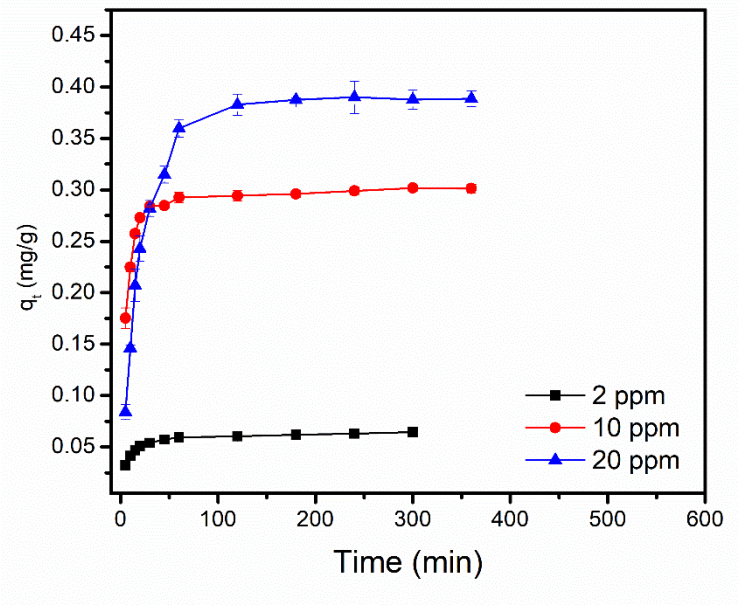

Figure 5. Variation of adsorption capacity (mg/g) with time. The adsorption reached equilibrium for t>120, t>180 and t>240 min for 2, 10 and 20 ppm, respectively.

3.5 Kinetics of Se removal using the mathematically optimized beads. Figure 5 shows the variation of the adsorption capacity with adsorption time for the initial Se concentrations of 2, 10 and 20 ppm. These experiments were carried out at 25 ºC with the initial pH of 4 and bead dosage of 30 g/L. Samples were taken out at smaller time intervals until 90 minutes, where the highest adsorption rates were recorded for all three concentrations. Based on the graphs shown in Fig. 5, the adsorption reached the equilibrium for t>120, t>180 and t>240 min for 2, 10 and 20 ppm respectively, showing less than 2% difference of adsorption capacity compared to the subsequent sampling points. These data were further studied with two kinetic models: pseudo-first order and pseudo-second order, in order to gain a better understanding of the adsorption

process and possible adsorption mechanism. The linear forms of the pseudo-first order and pseudo-second order were used as previously described in the literature.[52-54] The linear fitting of the data is shown in ESI figure S5. The linear fitting was used to obtain the adsorption kinetics parameters and results are summarized in table 1. Here the experimental adsorption capacity, $q_{e,exp}$ and kinetic parameters are the average results of the experimental data. The best linear fits are shown in figure S5.

Table 1. Kinetic parameters from the adsorption kinetics models

Se conc., ppm	$q_{e,exp}$ (mg/g)	Pseudo-first order			Pseudo-second order		
		k_1 (min^{-1})	$q_{e,cal}$ (mg/g)	R^2	k_2 ($g \cdot mg^{-1}min^{-1}$)	$q_{e,exp}$ (mg/g)	R^2
2	0.063±0.003	0.039±0.002	0.032±0.003	0.959	3.0±0.5	0.0638±0.0004	0.999
10	0.300±0.002	0.02±0.01	0.08±0.01	0.966	1.0±0.3	0.30±0.01	0.999
20	0.40±0.01	0.024±0.002	0.329±0.002	0.995	0.10±0.01	0.439±0.002	0.995

The goodness of fit values close to unity indicates the pseudo-second order kinetic describes the adsorption process better. For the 20 ppm Se, the R^2 values were very close, however further justification of selection of a kinetic model can be done by comparing the experimental and calculated values for the adsorption capacity. Based on the calculated *p-values* of the two tailed t-test at α=0.05 for the experimental and calculated adsorption capacity, suitability of the pseudo-second order kinetic model was further justified. For the pseudo-first order kinetic model, *p-values* of < 0.0001 were obtained for all 2, 10 and 20 ppm, indicating that the calculated adsorption capacities are significantly different from the experimental values. The obtained *p-values* of 0.67 and 1.00 for 2 and 10 ppm, respectively, for the pseudo-second order kinetic model demonstrated agreement with the experimental values. However, for 20 ppm, the

calculated p value was <0.0001, indicating that the experimental value was significantly different from the calculated values with the pseudo-second order kinetic model. On the other hand, the calculated and experimental values were much closer for the pseudo-second order kinetic model than the pseudo-first order kinetic model. Based on the characteristics of the pseudo-second order kinetics model, it can be postulated that the rate-limiting step of the Se adsorption by CS-PEI-GO beads is a chemisorption process that involves strong chemical interaction between the Se species and the active sites on CS-PEI-GO beads.[52, 54, 77] It is possible that the Se species attached to the protonated -OH, -NH_2 and -COOH functional groups go through further complexations, making the adsorption process irreversible as indicated by the best fit with the pseudo-second order model. [53-54]

As evident from the XPS spectra of the used CS-PEI-GO beads given in figure 6. Selenium was successfully adsorbed by the beads generating a peak at 52 eV binding energy, which can be attributed to the Se 3d core level. The deconvolution of the C1s core level suggests that the -C-OH group were oxidized during the adsorption process indicating the existence of the redox reaction happening at the adsorption sites. Even though the binding of selenium oxyanion

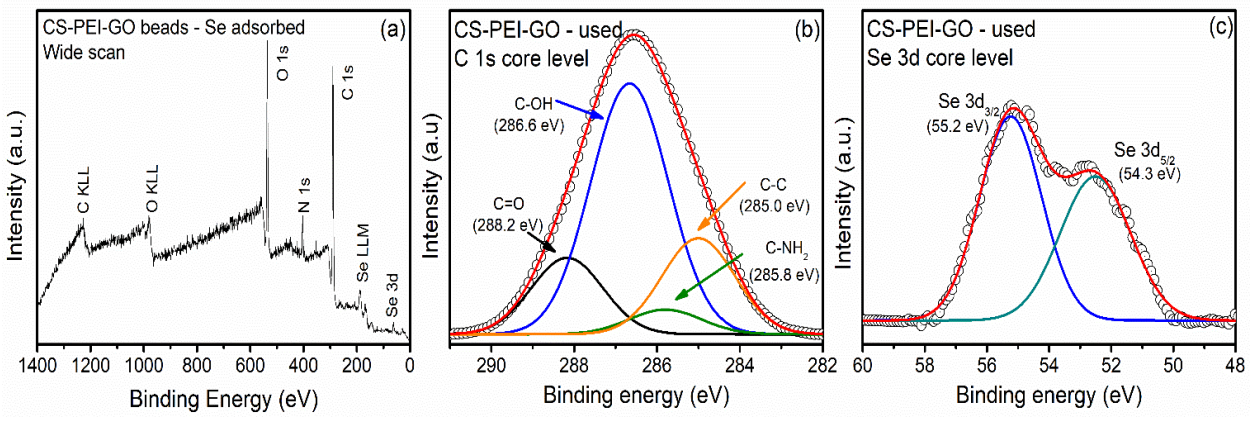

Figure 6. XPS spectra of spent CS-PEI-GO nanocomposite beads showing (a) wide scan (b) deconvolution of C1s core level suggests that the -C-OH group were oxidized during the adsorption process indicating the existence of the redox reaction happening at the adsorption sites, and (c) deconvolution of Se 3d core level shows successful adsorption by the beads.

455 species is a debatable topic to date, the obtained results suggest the adsorbed selenium has a
456 significant interaction towards the hydroxyl to form a chemical complex.[39, 41, 78] It is worth to
457 note that the reported mechanisms do not necessarily require protonation of alcoholic groups and
458 amine groups, which could be the underlying mechanism of Se uptake in higher pH values.
459 However, in the present study the removals with lower pH values were significantly higher
460 indicating that the electrostatic attraction due to protonation of alcoholic groups has a
461 predominant role in removing Se.[41, 59, 78]

462 **3.6 Adsorption isotherm studies for Se removal using the optimized beads.** Isotherm studies
463 were carried out at 25 ºC to investigate the Se adsorption properties. Qe vs Ce curves for initial
464 selenium concentrations of 5 to 250 ppm were fitted using non-linear forms of Langmuir and
465 Freundlich adsorption models as described earlier.[53, 55, 78-79] Obtained experimental data and non-
466 linear curve fits are shown in figure S6. The most statistically relevant isotherm model was
467 selected based on the goodness-of-fit, R^2, criterion. For the Langmuir isotherm, R^2 value of 0.995
468 was obtained; while R^2 of 0.998 was obtained for the Freundlich isotherm suggesting that both
469 isotherms might describe the adsorption process adequately as shown in earlier studies.[41, 55-56, 58]
470 Values obtained for the Freundlich isotherm: K_F and n were 0.093 L/g and 2.1, respectively;
471 while the values obtained for the Langmuir isotherm: b and Q_m were 0.01 L/g and 1.62 mg/g,
472 respectively. The maximum adsorption obtained in the present study is very competitive
473 compared to the other adsorbent materials found in the literature, as shown in the table 2.

474

475

476

Table 2. Comparison of maximum adsorption capacity with prior studies

Adsorbent material	Q_m (mg/g)
CS-PEI-GO beads (this work)	1.62
Magnetite[80]	0.22
Hematite[81]	0.39
Goethite[81]	0.52
Aluminium oxide coated sand[82]	1.08
Fe_3O_4-chitosan nanocomposite hollow fibres[83]	1.34
TiO_2[84]	1.64

With the premise of hydroxyl ions being the predominant functional group that is resulting in Se adsorption based on the XPS spectra observed earlier, it is fair to say the homogeneous monolayer adsorption suggested by the Langmuir isotherm might be a better model. As other studies have previously stated, it is also worth to note that the heterogeneous nature of the adsorption process suggested by the Freundlich isotherm agrees with the characteristics of the CS-PEI-GO beads, as they consist of various functional groups such as -OH, -COOH, and $-NH_2$ on the surface. Furthermore, protonated amine can be part of the selenium ion uptake during acidic conditions.[1, 39, 41, 56] This also suggests that there could be multiple functional groups; hence multiple underlying mechanisms undergoing during the Se adsorption.[41]

3.7 Regeneration of mathematically optimized beads. The spent CS-PEI-GO beads were used for regeneration studies employing four different desorption agents: 0.1 M HCl, 1 M HCl, 0.1 M NaOH and 1 M NaOH to investigate the possibility of regeneration of the active sites for

subsequent cycles of adsorption. Results obtained for four subsequent cycles are shown in figure 7.

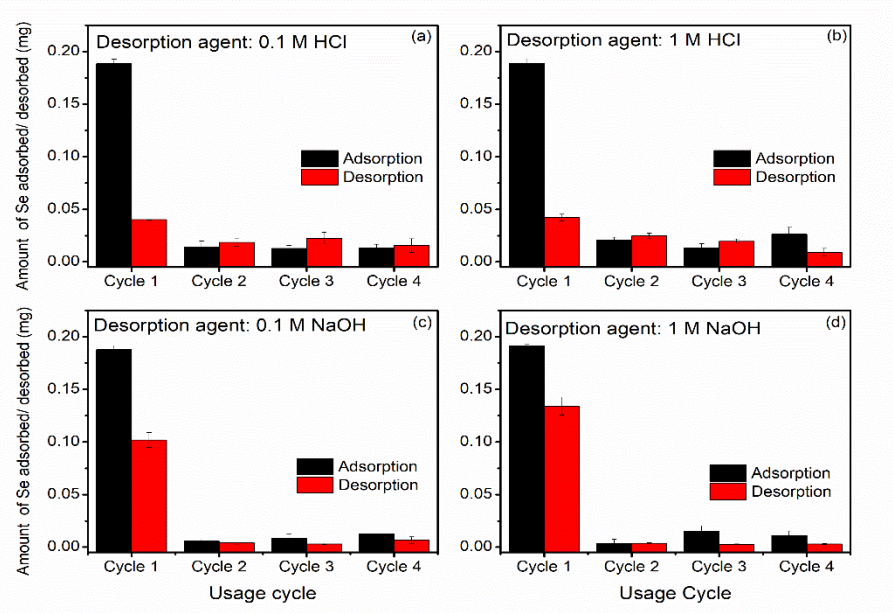

Figure 7. Amount of Se adsorbed/desorbed with (a) 0.1 M HCl, (b) 1 M HCl, (c) 0.1 M NaOH and (d) 1 M NaOH as desorption agents. Beads exposed to acidic desorption agents showed higher removals suggesting that the acidic nature of the desorption agent might be more effective in regenerating some active sites on the bead surface.

In the adsorption and desorption assays, the data were normalized by the bead dosage for each case. As shown in the figure 7c and 7d, 0.1 M NaOH and 1 M NaOH showed more efficient desorption of Se from the used beads with more than 50% of the adsorbed Se recovered. As suggested by the calculated p-values of 0.35, there was no significant difference in the amounts of Se desorbed by the 0.1 M HCl and 1 M HCl. Furthermore, these desorption approaches were significantly lower compared to the alkaline desorption agents used. Even though there were indications of desorption of Se, all the initial active sites responsible for the Se uptake were not regenerated as there were no significant removals recorded with any of the adsorption assays

after desorption. These results explain the findings of the adsorption kinetics, which suggested chemisorption as the main mechanism of Se uptake. In the chemisorption, the functional groups might undergo permanent changes making them unavailable for the reactions in subsequent adsorption cycles. Even though the removals were low, the beads exposed to acidic desorption agents showed marginally high removals indicating that the acidic nature of the desorption agent might be more effective in regenerating some active sites on the bead surface.

3.8 Application of beads with environmental samples spiked with selenium. The optimized beads were also tested against the Se spiked in real environmental water samples in order to mimic the potential applications of the beads. The batch adsorptions with bayou water and tap water samples were designed to represent the application of CS-PEI-GO beads for indirect potable reuse water treatment and simple water filtration for domestic point of use where excess amounts of Se in tap water has been recorded.[25-26, 85] The experiments were carried out at pH 4 and pH 7, as the pH was shown to be critical for Se removal efficiency and the results are illustrated in figure 8.

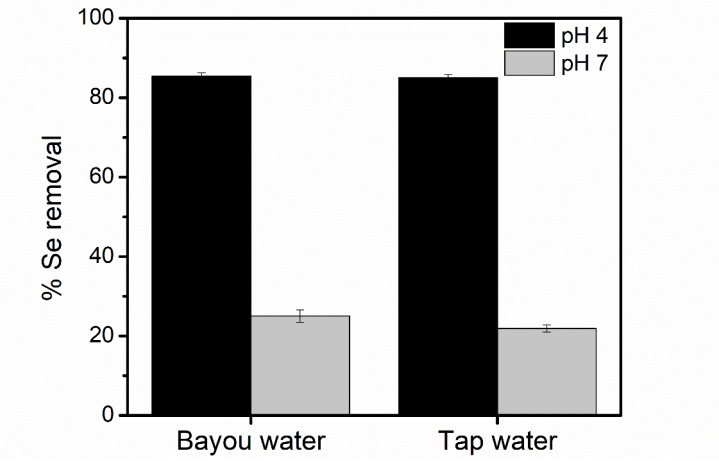

Figure 8. Percent Se removal with 10 ppm Se spiked bayou water and tap water at pH 4 and pH 7 also agrees with the observations made with pH earlier as Se removals were significantly high when initial pH is acidic.

Similar to the Se solutions made in DI water, the removals were more significant at pH 4 justifying the superior removals at acidic conditions. In terms of process development, this is important as the treatment of water for Se with CS-PEI-GO beads needs to be equipped with the additional pH controlling step for much better performance. In industrial scale, the pH controlling step could be easily applied to the water treatment process design, however, may not be suitable for domestic use. As of now, selenium can be removed using chemical reduction, coagulation-based processes and membrane separation processes, such as reverse osmosis and nanofiltration; however these approaches also have limitations.[41, 59, 86-87] Except for membrane processes, the other mentioned selenium removal methods depend on pH, and also result in large amounts of solid waste.[59, 86-87] However, based on the findings of the present study, it is worth to note that this can be overcome by increasing the availability of the adsorption sites by further adding more functional groups in the beads.

CONCLUSIONS

The RSM was successfully used to optimize a nanocomposite bead containing CS, PEI and GO for Se removal from water. A three-level BBD experimental design was used to model the system with three independent factors and % Se removal as the response variable. Mathematically optimized bead composition was experimentally validated showing that the inclusion of GO increased the Se removal significantly compared to the control beads. The optimized beads showed efficient Se removals in acidic conditions owing to the dissociations of selenous acid, which allowed protonation of functional groups from CS and GO, such as -OH and -COOH. These functional groups are known to uptake negatively charged heavy metal species.[1, 48, 88-89] The adsorption kinetic studies showed better agreement with the pseudo-second order kinetic models indicating the adsorption process is most likely a chemisorption process.

This was further corroborated by the regeneration studies showing that the spent adsorption sites are hard to regenerate as they undergo permanent changes making them unavailable for subsequent adsorption cycles. The beads were also tested with Se spiked bayou water samples and tap water samples indicating the acidic conditions were more suitable for Se removal as shown earlier. As the limitation of the Se removal by this novel material is governed by the solution pH and regeneration, it can be concluded that for more practical application of the CS-PEI-GO beads, this material should be directed towards increasing the availability of active sites by adding another polymer that would provide additional binding sites to adsorb Se.

ASSOCIATED CONTENT

Supporting information

Table S1 (Experimental factors and conditions used for the three-level Box-Behnken Design), Table S2 (Box-Behnken Design for Se removal), Figure S1 (Residual analysis), Figure S2 (Surface plots for Se removal), Figure S3 (Experimental validation of the optimized CS-PEI-GO beads), Figure S4 (Characterization of CS-PEI-GO beads), Figure S5 (Linear fitting of the data with the linearized forms of kinetic models), Figure S6 (Experimental isotherm data and non-linear isotherm model curve fits).

AUTHOR INFORMATION

Corresponding author

*Phone: +1 713-743-1495. E-mail: dfrigirodrigues@uh.edu

ORCID

Pasan C. Bandara: 0000-0001-7562-4377

Jem Valerie D. Perez: 0000-0002-0330-4806

Enrico T. Nadres: 0000-0002-7591-5868

Raj G. Nannapaneni: 0000-0002-4974-6810

Konrad J. Krakowiak: 0000-0003-0374-9554

Debora F. Rodrigues: 0000-0002-3124-1443

NOTES

The authors declare no competing financial interest.

ACKNOWLEDGEMENTS

This work was supported by the US Department of Interior, Bureau of Reclamation through the Desalination and Water Purification Research and Development Program (Agreement No. R16AC00123); CBET NSF Career grant number: 1150255; NSF BEINM Grant Number: 1705511, NSF CMMI Award Number: 1825921, as well as the Welch Foundation Award Number: E-2011-20190330. The findings achieved herein are solely the responsibility of the authors. Authors would like to extend their acknowledgements to Dr. Janire Peña Bahamonde, Dr. Haleh Ardebili, Dr. Charisma Lattao, Dr. Nalinda Kulatunga, and Sofia K. Fanourakis for their valuable contributions to the present study.

REFERENCES

(1) Perez, J. V. D.; Nadres, E. T.; Nguyen, H. N.; Dalida, M. L. P.; Rodrigues, D. F. Response surface methodology as a powerful tool to optimize the synthesis of polymer-based graphene oxide nanocomposites for simultaneous removal of cationic and anionic heavy metal contaminants. *RSC Advances* **2017,** *7* (30), 18480-18490, DOI: 10.1039/C7RA00750G.

(2) Perreault, F.; Fonseca de Faria, A.; Elimelech, M. Environmental applications of graphene-based nanomaterials. *Chemical Society Reviews* **2015,** *44* (16), 5861-5896, DOI: 10.1039/C5CS00021A.
(3) Westerhoff, P.; Alvarez, P.; Li, Q.; Gardea-Torresdey, J.; Zimmerman, J. Overcoming implementation barriers for nanotechnology in drinking water treatment. *Environmental Science: Nano* **2016,** *3* (6), 1241-1253, DOI: 10.1039/C6EN00183A.
(4) Mauter, M. S.; Zucker, I.; Perreault, F.; Werber, J. R.; Kim, J.-H.; Elimelech, M. The role of nanotechnology in tackling global water challenges. *Nature Sustainability* **2018,** *1* (4), 166-175, DOI: 10.1038/s41893-018-0046-8.
(5) Xie, Y.; Chen, C.; Ren, X.; Wang, X.; Wang, H.; Wang, X. Emerging natural and tailored materials for uranium-contaminated water treatment and environmental remediation. *Progress in Materials Science* **2019,** *103*, 180-234.
(6) Kuilla, T.; Bhadra, S.; Yao, D.; Kim, N. H.; Bose, S.; Lee, J. H. Recent advances in graphene based polymer composites. *Progress in Polymer Science* **2010,** *35* (11), 1350-1375, DOI: https://doi.org/10.1016/j.progpolymsci.2010.07.005.
(7) Palencia, C.; Rubio, J.; Rubio, F.; Fierro, J. L. G.; Oteo, J. L. Silane Coupling Agent Structures on Carbon Nanofibers. *Journal of Nanoscience and Nanotechnology* **2011,** *11* (5), 4142-4152, DOI: 10.1166/jnn.2011.4147.
(8) Yu, K.; Ho, J.; McCandlish, E.; Buckley, B.; Patel, R.; Li, Z.; Shapley, N. C. Copper ion adsorption by chitosan nanoparticles and alginate microparticles for water purification applications. *Colloids and Surfaces A: Physicochemical and Engineering Aspects* **2013,** *425*, 31-41, DOI: https://doi.org/10.1016/j.colsurfa.2012.12.043.
(9) Filipkowska, U.; Jóźwiak, T. *Application of chemically-cross-linked chitosan for the removal of Reactive Black 5 and Reactive Yellow 84 dyes from aqueous solutions*, 2013; Vol. 33, p 735-747.
(10) Wu, F.-C.; Tseng, R.-L.; Juang, R.-S. A review and experimental verification of using chitosan and its derivatives as adsorbents for selected heavy metals. *Journal of Environmental Management* **2010,** *91* (4), 798-806, DOI: https://doi.org/10.1016/j.jenvman.2009.10.018.
(11) Bailey, S. E.; Olin, T. J.; Bricka, R. M.; Adrian, D. D. A review of potentially low-cost sorbents for heavy metals. *Water Research* **1999,** *33* (11), 2469-2479, DOI: https://doi.org/10.1016/S0043-1354(98)00475-8.
(12) Medina, R. P.; Nadres, E. T.; Ballesteros, F. C.; Rodrigues, D. F. Incorporation of graphene oxide into a chitosan–poly(acrylic acid) porous polymer nanocomposite for enhanced lead adsorption. *Environmental Science: Nano* **2016,** *3* (3), 638-646, DOI: 10.1039/C6EN00021E.
(13) Li, N.; Bai, R. A Novel Amine-Shielded Surface Cross-Linking of Chitosan Hydrogel Beads for Enhanced Metal Adsorption Performance. *Industrial & Engineering Chemistry Research* **2005,** *44* (17), 6692-6700, DOI: 10.1021/ie050145k.
(14) Li, X.; Zhou, H.; Wu, W.; Wei, S.; Xu, Y.; Kuang, Y. Studies of heavy metal ion adsorption on Chitosan/Sulfydryl-functionalized graphene oxide composites. *Journal of Colloid and Interface Science* **2015,** *448*, 389-397, DOI: https://doi.org/10.1016/j.jcis.2015.02.039.
(15) Deng, S.; Ting, Y. P. Polyethylenimine-Modified Fungal Biomass as a High-Capacity Biosorbent for Cr(VI) Anions: Sorption Capacity and Uptake Mechanisms. *Environmental Science & Technology* **2005,** *39* (21), 8490-8496, DOI: 10.1021/es050697u.
(16) Virgen-Ortíz, J. J.; dos Santos, J. C. S.; Berenguer-Murcia, Á.; Barbosa, O.; Rodrigues, R. C.; Fernandez-Lafuente, R. Polyethylenimine: a very useful ionic polymer in the design of

627 immobilized enzyme biocatalysts. *Journal of Materials Chemistry B* **2017,** *5* (36), 7461-7490,
628 DOI: 10.1039/C7TB01639E.
629 (17) Zhang, X.; Lin, D.; Chen, W. Nitrogen-doped porous carbon prepared from a liquid carbon
630 precursor for CO2 adsorption. *RSC Advances* **2015,** *5* (56), 45136-45143, DOI:
631 10.1039/C5RA08014B.
632 (18) Basu, R.; Haque, S. E.; Tang, J.; Ji, J.; Johannesson, K. H. Evolution of selenium
633 concentrations and speciation in groundwater flow systems: Upper Floridan (Florida) and
634 Carrizo Sand (Texas) aquifers. *Chemical Geology* **2007,** *246* (3), 147-169, DOI:
635 https://doi.org/10.1016/j.chemgeo.2007.09.010.
636 (19) Korobova, E. M.; Ryzhenko, B. N.; Cherkasova, E. V.; Sedykh, E. M.; Korsakova, N. V.;
637 Danilova, V. N.; Khushvakhtova, S. D.; Berezkin, V. Y. Iodine and selenium speciation in
638 natural waters and their concentrating at landscape-geochemical barriers. *Geochemistry*
639 *International* **2014,** *52* (6), 500-514, DOI: http://dx.doi.org/10.1134/S001670291404003X.
640 (20) Zawislanski, P. T.; Benson, S. M.; TerBerg, R.; Borglin, S. E. Selenium Speciation,
641 Solubility, and Mobility in Land-Disposed Dredged Sediments. *Environmental Science &*
642 *Technology* **2003,** *37* (11), 2415-2420, DOI: 10.1021/es020977z.
643 (21) Peter W. Bush, A. F. A., Lynne Fahlquist, Patricia B. Ging, C. Evan Hornig, Jennifer
644 Lanning-Rush *Water Quality in South-Central Texas* US Geological Survey: 2000.
645 (22) Robert, C. R., Bridget R. Scanlon, Steven Walden, Gil Strassbery *Naturally occuring*
646 *groundwater contamination in Texas*; Texas Water Development Board: 2011.
647 (23) Effiong Ukorebi, E. Occurrence and Distribution of Arsenic, Antimony and Selenium in
648 Shallow Groundwater Systems of Ibadan Metropolis, Southwestern Nigerian. *Journal of Health*
649 *and Pollution* **2017,** *7* (13), 32-41, DOI: 10.5696/2156-9614-7.13.32.
650 (24) Kuisi, M. A.; Abdel-fattah, A. Groundwater vulnerability to selenium in semi-arid
651 environments: Amman Zarqa Basin, Jordan. *Environmental Geochemistry and Health* **2010,** *32*
652 (2), 107-28, DOI: http://dx.doi.org/10.1007/s10653-009-9269-y.
653 (25) Vinceti, M.; Bonvicini, F.; Rothman, K. J.; Vescovi, L.; Wang, F. The relation between
654 amyotrophic lateral sclerosis and inorganic selenium in drinking water: a population-based case-
655 control study. *Environmental Health* **2010,** *9* (1), 77, DOI: 10.1186/1476-069X-9-77.
656 (26) Vinceti, M.; Cann, C. I.; Calzolari, E.; Vivoli, R.; Garavelli, L.; Bergomi, M. Reproductive
657 outcomes in a population exposed long-term to inorganic selenium via drinking water. *Science of*
658 *The Total Environment* **2000,** *250* (1), 1-7, DOI: https://doi.org/10.1016/S0048-9697(99)00419-
659 2.
660 (27) Igarashi, T.; Sasaki, R.; Tabelin, C. B. Chemical Forms of Arsenic and Selenium Leached
661 from Mudstones. *Procedia Earth and Planetary Science* **2013,** *6*, 105-113, DOI:
662 https://doi.org/10.1016/j.proeps.2013.01.015.
663 (28) Tabelin, C. B.; Hashimoto, A.; Igarashi, T.; Yoneda, T. Leaching of boron, arsenic and
664 selenium from sedimentary rocks: I. Effects of contact time, mixing speed and liquid-to-solid
665 ratio. *Science of The Total Environment* **2014,** *472*, 620-629, DOI:
666 https://doi.org/10.1016/j.scitotenv.2013.11.006.
667 (29) National Primary Drinking Water Regulaion Table. In *EPA 816-F-09-004*, Agency, U. S. E.
668 P., Ed. 2009; p 7.
669 (30) Project, E. I. *Don't Drink the Water*; Environmental Integrity Project: 2016.
670 (31) Vinceti, M.; Crespi, C. M.; Bonvicini, F.; Malagoli, C.; Ferrante, M.; Marmiroli, S.;
671 Stranges, S. The need for a reassessment of the safe upper limit of selenium in drinking water.

Science of The Total Environment **2013,** *443*, 633-642, DOI: https://doi.org/10.1016/j.scitotenv.2012.11.025.
(32) Ackerman, J. T.; Eagles-Smith, C. A.; Herzog, M. P.; Hartman, C. A. Maternal transfer of contaminants in birds: Mercury and selenium concentrations in parents and their eggs. *Environmental Pollution* **2016,** *210*, 145-154, DOI: https://doi.org/10.1016/j.envpol.2015.12.016.
(33) Brady, C.; Petrie, S.; Schummer, M.; Badzinski, S.; Belzile, N.; Chen, Y.-W. Effects of dietary selenium on the health and survival of captive wintering lesser scaup. *Environmental Pollution* **2013,** *175*, 8-15, DOI: https://doi.org/10.1016/j.envpol.2012.12.005.
(34) King, K. A.; Custer, T. W.; Weaver, D. A. Reproductive success of barn swallows nesting near a selenium-contaminated lake in east Texas, USA. *Environmental Pollution* **1994,** *84* (1), 53-58, DOI: https://doi.org/10.1016/0269-7491(94)90070-1.
(35) Lindsay, L. W.; Scott, A. P.; Robert, C. B.; Shannon, S. B.; Michael, L. S.; Yu-Wei, C.; Nelson, B. Effects of Elevated Selenium on Body Condition, Oxidative Stress, and Organ Health in Greater Scaup Wintering at Lake Ontario. *Wildlife Society Bulletin (2011-)* **2012,** *36* (3), 506-511.
(36) Loguercio, C.; De Girolamo, V.; Federico A, A.; Feng, S. L.; Cataldi, V.; Del Vecchio Blanco, C.; Gialanella, G. Trace Elements and Chronic Liver Diseases. *Journal of Trace Elements in Medicine and Biology* **1997,** *11* (3), 158-161, DOI: https://doi.org/10.1016/S0946-672X(97)80045-4.
(37) Li, J.; Wang, X.; Zhao, G.; Chen, C.; Chai, Z.; Alsaedi, A.; Hayat, T.; Wang, X. Metal–organic framework-based materials: superior adsorbents for the capture of toxic and radioactive metal ions. *Chemical Society Reviews* **2018,** *47* (7), 2322-2356, DOI: 10.1039/C7CS00543A.
(38) Cui, W.; Li, P.; Wang, Z.; Zheng, S.; Zhang, Y. Adsorption study of selenium ions from aqueous solutions using MgO nanosheets synthesized by ultrasonic method. *Journal of Hazardous Materials* **2018,** *341*, 268-276, DOI: https://doi.org/10.1016/j.jhazmat.2017.07.073.
(39) Xiao, W.; Yan, B.; Zeng, H.; Liu, Q. Dendrimer functionalized graphene oxide for selenium removal. *Carbon* **2016,** *105*, 655-664, DOI: https://doi.org/10.1016/j.carbon.2016.04.057.
(40) Holmes, A. B.; Gu, F. X. Emerging nanomaterials for the application of selenium removal for wastewater treatment. *Environmental Science: Nano* **2016,** *3* (5), 982-996, DOI: 10.1039/C6EN00144K.
(41) Fu, Y.; Wang, J.; Liu, Q.; Zeng, H. Water-dispersible magnetic nanoparticle–graphene oxide composites for selenium removal. *Carbon* **2014,** *77*, 710-721, DOI: https://doi.org/10.1016/j.carbon.2014.05.076.
(42) Lu, H.; Zhang, S.; Guo, L.; Li, W. Applications of graphene-based composite hydrogels: a review. *RSC Advances* **2017,** *7* (80), 51008-51020, DOI: 10.1039/C7RA09634H.
(43) Yu, Y.; Andrade, L.; Fang, L.; Ma, J.; Zhang, W.; Tang, Y. Graphene oxide and hyperbranched polymer-toughened hydrogels with improved absorption properties and durability. *Journal of Materials Science* **2015,** *50* (9), 3457-3466, DOI: 10.1007/s10853-015-8905-4.
(44) Chen, Y.; Chen, L.; Bai, H.; Li, L. Graphene oxide–chitosan composite hydrogels as broad-spectrum adsorbents for water purification. *Journal of Materials Chemistry A* **2013,** *1* (6), 1992-2001, DOI: 10.1039/C2TA00406B.
(45) Liu, J.; Zhu, K.; Jiao, T.; Xing, R.; Hong, W.; Zhang, L.; Zhang, Q.; Peng, Q. Preparation of graphene oxide-polymer composite hydrogels via thiol-ene photopolymerization as efficient dye

adsorbents for wastewater treatment. *Colloids and Surfaces A: Physicochemical and Engineering Aspects* **2017,** *529*, 668-676, DOI: https://doi.org/10.1016/j.colsurfa.2017.06.050.
(46) Liao, G.; Hu, J.; Chen, Z.; Zhang, R.; Wang, G.; Kuang, T. Preparation, Properties, and Applications of Graphene-Based Hydrogels. *Front Chem* **2018,** *6*, 450-450, DOI: 10.3389/fchem.2018.00450.
(47) Hummers, W. S.; Offeman, R. E. Preparation of Graphitic Oxide. *Journal of the American Chemical Society* **1958,** *80* (6), 1339-1339, DOI: 10.1021/ja01539a017.
(48) Bandara, P. C.; Nadres, E. T.; Rodrigues, D. F. Use of Response Surface Methodology To Develop and Optimize the Composition of a Chitosan–Polyethyleneimine–Graphene Oxide Nanocomposite Membrane Coating To More Effectively Remove Cr(VI) and Cu(II) from Water. *ACS Applied Materials & Interfaces* **2019,** *11* (19), 17784-17795, DOI: 10.1021/acsami.9b03601.
(49) Marcano, D. C.; Kosynkin, D. V.; Berlin, J. M.; Sinitskii, A.; Sun, Z.; Slesarev, A.; Alemany, L. B.; Lu, W.; Tour, J. M. Improved Synthesis of Graphene Oxide. *ACS Nano* **2010,** *4* (8), 4806-4814, DOI: 10.1021/nn1006368.
(50) Hou, J.; Dong, G.; Ye, Y.; Chen, V. Enzymatic degradation of bisphenol-A with immobilized laccase on TiO2 sol–gel coated PVDF membrane. *Journal of Membrane Science* **2014,** *469* (2015), 19-30.
(51) Barrett, E. P.; Joyner, L. G.; Halenda, P. P. The Determination of Pore Volume and Area Distributions in Porous Substances. I. Computations from Nitrogen Isotherms. *Journal of the American Chemical Society* **1951,** *73* (1), 373-380, DOI: 10.1021/ja01145a126.
(52) Largitte, L.; Pasquier, R. A review of the kinetics adsorption models and their application to the adsorption of lead by an activated carbon. *Chemical Engineering Research and Design* **2016,** *109*, 495-504, DOI: https://doi.org/10.1016/j.cherd.2016.02.006.
(53) Nethaji, S.; Sivasamy, A.; Mandal, A. B. Adsorption isotherms, kinetics and mechanism for the adsorption of cationic and anionic dyes onto carbonaceous particles prepared from Juglans regia shell biomass. *International Journal of Environment Science and Technology* **2013,** *10* (2), DOI: 10.1007/s13762-012-0112-0.
(54) Ho, Y. S.; McKay, G. Pseudo-second order model for sorption processes. *Process Biochemistry* **1999,** *34* (5), 451-465, DOI: https://doi.org/10.1016/S0032-9592(98)00112-5.
(55) Kailas, L. W.; Prasad, B.; Ch. Sekhararao, G. BATCH STUDY, EQUILIBIRUM AND KINETICS OF ADSORPTION OF SELENIUM USING RICE HUSK ASH (RHA). *Journal of Engineering Science and Technology* **2011,** *6* (5), 586-605.
(56) Jegadeesan, G. B.; Mondal, K.; Lalvani, S. B. Adsorption of Se (IV) and Se (VI) Using Copper-Impregnated Activated Carbon and Fly Ash-Extracted Char Carbon. *Water, Air, & Soil Pollution* **2015,** *226* (8), 234, DOI: 10.1007/s11270-015-2520-5.
(57) Sarkar, M.; Majumdar, P. Application of response surface methodology for optimization of heavy metal biosorption using surfactant modified chitosan bead. *Chemical Engineering Journal* **2011,** *175*, 376-387, DOI: https://doi.org/10.1016/j.cej.2011.09.125.
(58) Wasewar, K. L.; Prasad, B.; Gulipalli, S. Removal of Selenium by Adsorption onto Granular Activated Carbon (GAC) and Powdered Activated Carbon (PAC). *CLEAN – Soil, Air, Water* **2009,** *37* (11), 872-883, DOI: 10.1002/clen.200900188.
(59) Santos, S.; Ungureanu, G.; Boaventura, R.; Botelho, C. Selenium contaminated waters: An overview of analytical methods, treatment options and recent advances in sorption methods. *Science of The Total Environment* **2015,** *521-522*, 246-260, DOI: https://doi.org/10.1016/j.scitotenv.2015.03.107.

(60) Thommes, M.; Kaneko, K.; Neimark Alexander, V.; Olivier James, P.; Rodriguez-Reinoso, F.; Rouquerol, J.; Sing Kenneth, S. W., Physisorption of gases, with special reference to the evaluation of surface area and pore size distribution (IUPAC Technical Report). In *Pure and Applied Chemistry*, 2015; Vol. 87, p 1051.
(61) Alkhamis, K. A.; Salem, M. S.; Khanfar, M. S. The sorption of ketotifen fumarate by chitosan. *AAPS PharmSciTech* **2008,** *9* (3), 866-869, DOI: 10.1208/s12249-008-9123-z.
(62) Arabyarmohammadi, H.; Darban, A. K.; Abdollahy, M.; Yong, R.; Ayati, B.; Zirakjou, A.; van der Zee, S. E. A. T. M. Utilization of a Novel Chitosan/Clay/Biochar Nanobiocomposite for Immobilization of Heavy Metals in Acid Soil Environment. *Journal of Polymers and the Environment* **2018,** *26* (5), 2107-2119, DOI: 10.1007/s10924-017-1102-6.
(63) Li, Z.; Song, X.; Cui, S.; Jiao, Y.; Zhou, C. Fabrication of macroporous reduced graphene oxide composite aerogels reinforced with chitosan for high bilirubin adsorption. *RSC Advances* **2018,** *8* (15), 8338-8348, DOI: 10.1039/C8RA00358K.
(64) Mohanasrinivasan, V.; Mishra, M.; Paliwal, J. S.; Singh, S. K.; Selvarajan, E.; Suganthi, V.; Subathra Devi, C. Studies on heavy metal removal efficiency and antibacterial activity of chitosan prepared from shrimp shell waste. *3 Biotech* **2014,** *4* (2), 167-175, DOI: 10.1007/s13205-013-0140-6.
(65) Julkapli, N. M.; Ahmad, Z.; Akil, H. M. X-Ray Diffraction Studies of Cross Linked Chitosan With Different Cross Linking Agents For Waste Water Treatment Application. *AIP Conference Proceedings* **2010,** *1202* (1), 106-111, DOI: 10.1063/1.3295578.
(66) Zhang, Q.; Du, Q.; Hua, M.; Jiao, T.; Gao, F.; Pan, B. Sorption Enhancement of Lead Ions from Water by Surface Charged Polystyrene-Supported Nano-Zirconium Oxide Composites. *Environmental Science & Technology* **2013,** *47* (12), 6536-6544, DOI: 10.1021/es400919t.
(67) Wang, K.; Zhang, X.; Zhang, X.; Yang, B.; Li, Z.; Zhang, Q.; Huang, Z.; Wei, Y. One-pot preparation of cross-linked amphiphilic fluorescent polymer based on aggregation induced emission dyes. *Colloids and Surfaces B: Biointerfaces* **2015,** *126*, 273-279, DOI: https://doi.org/10.1016/j.colsurfb.2014.12.025.
(68) Grande Carlos, D.; Mangadlao, J.; Fan, J.; De Leon, A.; Delgado-Ospina, J.; Rojas Juan, G.; Rodrigues Debora, F.; Advincula, R. Chitosan Cross-Linked Graphene Oxide Nanocomposite Films with Antimicrobial Activity for Application in Food Industry. *Macromolecular Symposia* **2017,** *374* (1), 1600114, DOI: 10.1002/masy.201600114.
(69) López-Pérez, P. M.; Marques, A. P.; Silva, R. M. P. d.; Pashkuleva, I.; Reis, R. L. Effect of chitosan membrane surface modification via plasma induced polymerization on the adhesion of osteoblast-like cells. *Journal of Materials Chemistry* **2007,** *17* (38), 4064-4071, DOI: 10.1039/B707326G.
(70) Wang, Y.; Li, B.; Zhou, Y.; Jia, D. In Situ Mineralization of Magnetite Nanoparticles in Chitosan Hydrogel. *Nanoscale Research Letters* **2009,** *4* (9), 1041, DOI: 10.1007/s11671-009-9355-1.
(71) Yu Shu-juan, C. K., Wang Feng, Zhu Yong-fei. Synthesis of chitosan-based polymer carbon dots fluorescent materials and application of self-assembled drug-loading. *Chinese Optics* **2018,** *11* (3), 420-430.
(72) Duc, M.; Lefèvre, G.; Fédoroff, M. Sorption of selenite ions on hematite. *Journal of Colloid and Interface Science* **2006,** *298* (2), 556-563, DOI: https://doi.org/10.1016/j.jcis.2006.01.029.
(73) Dobrowolski, R.; Otto, M. Preparation and evaluation of Fe-loaded activated carbon for enrichment of selenium for analytical and environmental purposes. *Chemosphere* **2013,** *90* (2), 683-690, DOI: https://doi.org/10.1016/j.chemosphere.2012.09.049.

(74) Wang, X.; Chen, L.; Wang, L.; Fan, Q.; Pan, D.; Li, J.; Chi, F.; Xie, Y.; Yu, S.; Xiao, C.; Luo, F.; Wang, J.; Wang, X.; Chen, C.; Wu, W.; Shi, W.; Wang, S.; Wang, X. Synthesis of novel nanomaterials and their application in efficient removal of radionuclides. *Science China Chemistry* **2019,** *62* (8), 933-967, DOI: 10.1007/s11426-019-9492-4.
(75) Nie, Y.; Deng, S.; Wang, B.; Huang, J.; Yu, G. Removal of clofibric acid from aqueous solution by polyethylenimine-modified chitosan beads. *Frontiers of Environmental Science & Engineering* **2014,** *8* (5), 675-682, DOI: 10.1007/s11783-013-0622-0.
(76) Avadiar, L.; Leong, Y.-K. Interactions of PEI (polyethylenimine)--silica particles with citric acid in dispersions. *Colloid & Polymer Science* **2011,** *289* (3), 237-245, DOI: http://dx.doi.org/10.1007/s00396-010-2351-2.
(77) Simonin, J.-P. On the comparison of pseudo-first order and pseudo-second order rate laws in the modeling of adsorption kinetics. *Chemical Engineering Journal* **2016,** *300*, 254-263, DOI: https://doi.org/10.1016/j.cej.2016.04.079.
(78) Lu, Z.; Yu, J.; Zeng, H.; Liu, Q. Polyamine-modified magnetic graphene oxide nanocomposite for enhanced selenium removal. *Separation and Purification Technology* **2017,** *183*, 249-257, DOI: https://doi.org/10.1016/j.seppur.2017.04.010.
(79) Gong, X.; Li, W.; Wang, K.; Hu, J. Study of the adsorption of Cr(VI) by tannic acid immobilised powdered activated carbon from micro-polluted water in the presence of dissolved humic acid. *Bioresource Technology* **2013,** *141*, 145-151, DOI: https://doi.org/10.1016/j.biortech.2013.01.166.
(80) Martinez, M.; Gimenez, J.; Pablo, J. d.; Rovira, M.; Duro, L. Sorption of selenium(IV) and selenium(VI) onto magnetite. *Applied Surface Science* **2006,** *252* (10), 3767-3773, DOI: DOI:101016/japsusc200505067.
(81) Rovira, M.; Giménez, J.; Martínez, M.; Martínez-Lladó, X.; de Pablo, J.; Martí, V.; Duro, L. Sorption of selenium(IV) and selenium(VI) onto natural iron oxides: Goethite and hematite. *Journal of Hazardous Materials* **2008,** *150* (2), 279-284, DOI: https://doi.org/10.1016/j.jhazmat.2007.04.098.
(82) Kuan, W.-H.; Lo, S.-L.; Wang, M. K.; Lin, C.-F. Removal of Se(IV) and Se(VI) from water by aluminum-oxide-coated sand. *Water Research* **1998,** *32* (3), 915-923, DOI: https://doi.org/10.1016/S0043-1354(97)00228-5.
(83) Seyed Dorraji, M. S.; Amani-Ghadim, A. R.; Hanifehpour, Y.; Woo Joo, S.; Figoli, A.; Carraro, M.; Tasselli, F. Performance of chitosan based nanocomposite hollow fibers in the removal of selenium(IV) from water. *Chemical Engineering Research and Design* **2017,** *117*, 309-317, DOI: https://doi.org/10.1016/j.cherd.2016.10.043.
(84) Svecova, L.; Dossot, M.; Cremel, S.; Simonnot, M.-O.; Sardin, M.; Humbert, B.; Den Auwer, C.; Michot, L. J. Sorption of selenium oxyanions on TiO2 (rutile) studied by batch or column experiments and spectroscopic methods. *Journal of Hazardous Materials* **2011,** *189* (3), 764-772, DOI: https://doi.org/10.1016/j.jhazmat.2011.02.090.
(85) Petrini, R.; Slejko, F.; Lutman, A.; Pison, S.; Franceschini, G.; Zini, L.; Italiano, F.; Galic, A. Natural arsenic contamination in waters from the Pesariis village, NE Italy. *Environmental Earth Sciences* **2011,** *62* (3), 481-491, DOI: http://dx.doi.org/10.1007/s12665-010-0541-3.
(86) Richards, L. A.; Richards, B. S.; Schäfer, A. I. Renewable energy powered membrane technology: Salt and inorganic contaminant removal by nanofiltration/reverse osmosis. *Journal of Membrane Science* **2011,** *369* (1), 188-195, DOI: https://doi.org/10.1016/j.memsci.2010.11.069.

(87) Subramani, A.; Cryer, E.; Liu, L.; Lehman, S.; Ning, R. Y.; Jacangelo, J. G. Impact of intermediate concentrate softening on feed water recovery of reverse osmosis process during treatment of mining contaminated groundwater. *Separation and Purification Technology* **2012,** *88*, 138-145, DOI: https://doi.org/10.1016/j.seppur.2011.12.010.
(88) Pasan Chinthana Bandara, E. T. N., Debora Frigi Rodrigues. Use of response surface methodology to develop and optimize graphene oxide based nanocomposite membrane coatings for Cr(VI) and Cu(II) removal from water. *ACS Applied Materials & Interfaces* **2019**.
(89) Bandara, P. C.; Nadres, E. T.; Rodrigues, D. F. Use of response surface methodology to develop and optimize the composition of a chitosan-polyethyleneimine-graphene oxide nanocomposite membrane coating to more effectively remove Cr(VI) and Cu(II) from water. *ACS Applied Materials & Interfaces* **2019**, DOI: 10.1021/acsami.9b03601.